Supplemental Figures and Legends

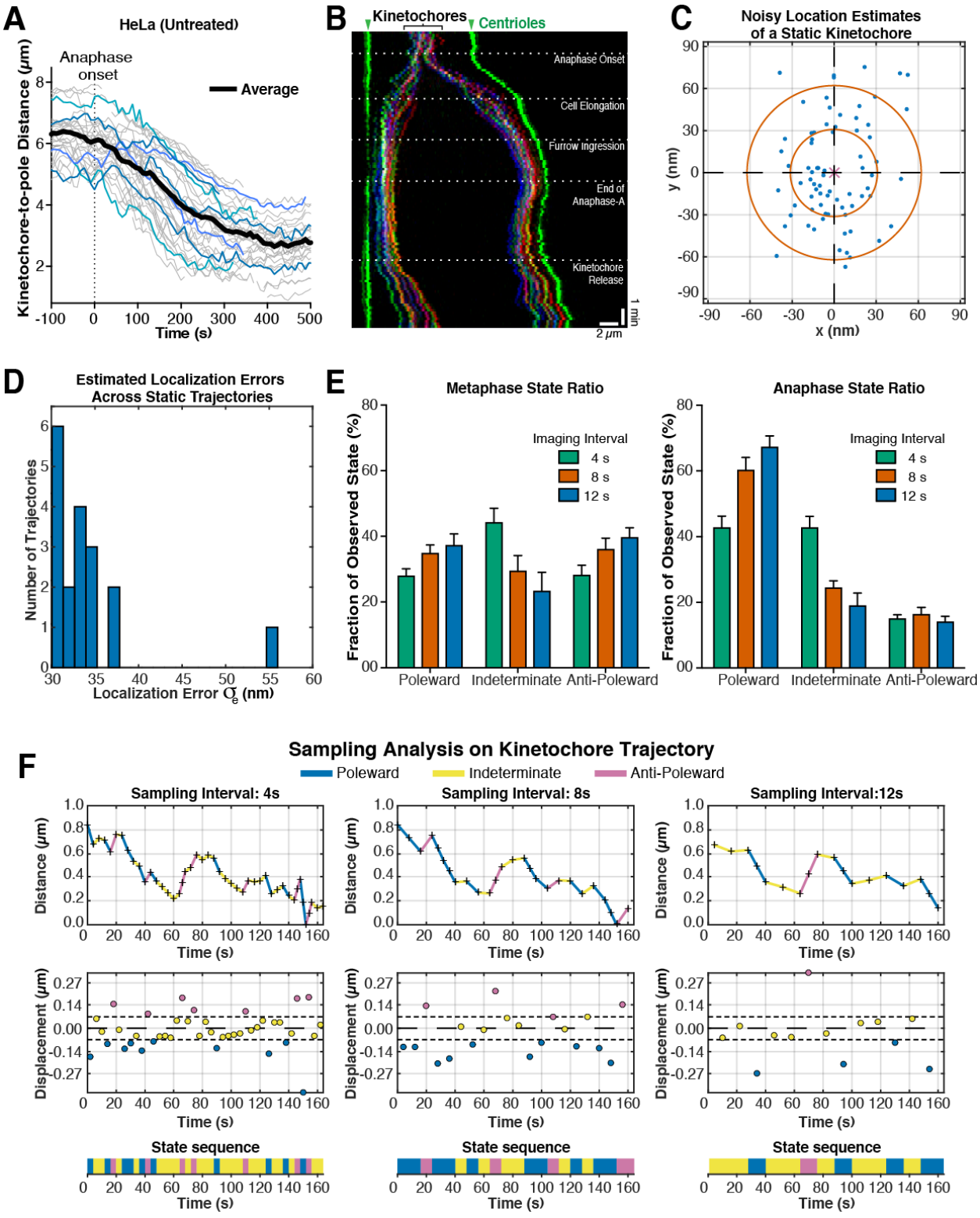

Figure S1. Characterization of anaphase chromosome dynamics from single-particle tracking and trajectory analysis. Related to Figure 1. (A) Kinetochore-to-pole distances for an example untreated HeLa cell. Representative distance trajectories over time are labeled in blue. The average distance measured over all trajectories in this cell over time is depicted by the bold black line. Anaphase onset is labeled as t = 0. (B) Color-coded kymograph of the time-lapse movie corresponding to Figure 1D aligned to one pole. The dashed lines indicate distinct anaphase events from sister chromatid separation onwards. (C) Example serial localizations from a single kinetochore tracked in a fixed HeLa cell (solid blue dots) plotted together with the mean position of the kinetochore (magenta 'x') determined from the average of the serial kinetochore localizations. Red circles denote successive standard deviations from the mean measured by a normal distribution fitted to the localizations. The estimated localization error for this single kinetochore corresponds to the standard deviation. (D) Histogram of localization errors estimated from multiple kinetochores as depicted in Figure S1C. The localization error determined from this fixed cell (n = 18 kinetochores) was 34.2 ± 5.8 nm (mean ± s.d.). (E) State ratio comparison of untreated HeLa cells during metaphase (left) or anaphase (right) imaged at 4 second intervals and subsequently coarsened to 8 and 12 second intervals by omitting successive time-frames (n=8 cells). (F) Example kinetochore distance trajectory in anaphase imaged at 4 seconds/frame. Top: relative distance of the kinetochore from its spindle pole over the entire observed trajectory. Each curve is annotated using colors that denote the state of motion of the kinetochore during the corresponding interval. Middle: displacements (change in distance between successive time points) along the distance trajectory. The top and bottom dotted lines denote the localization error threshold that determines whether kinetochore motion is classified as poleward/anti-poleward or indeterminate. A positive displacement represents an anti-poleward motion in this regime (an increase in distance from the spindle pole). Bottom: the state sequence, or series of annotations of poleward/anti-poleward/indeterminate kinetochore motions, at successive time points in the trajectory. From left to right, the temporal sampling of the original trajectory is "coarsened" computationally from the original experimental imaging time sampling of 4 seconds/frame to 8 and 12 seconds/frame to test the role of temporal sampling on motion classification.

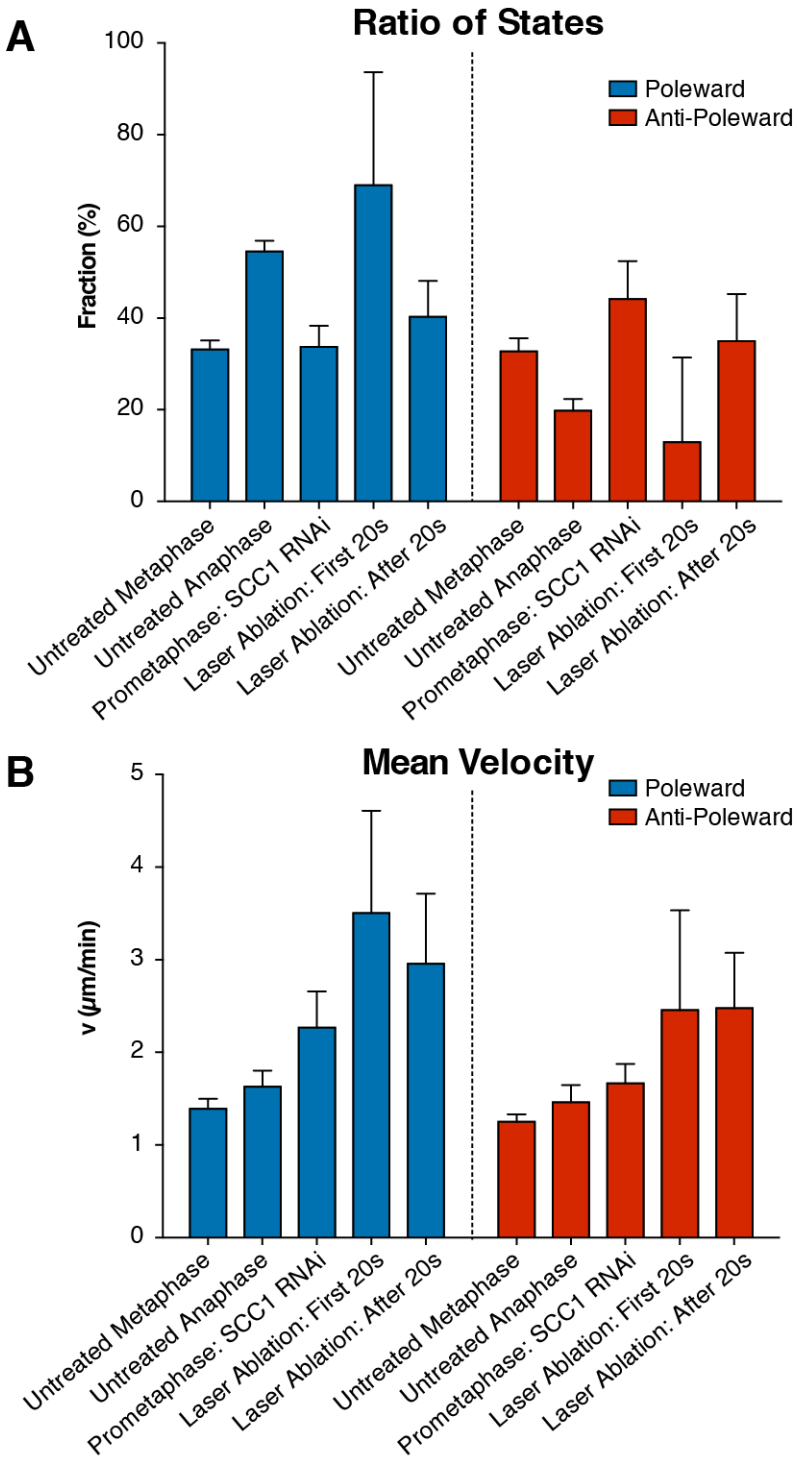

Figure S2. Effects of removal of physical connections between sister chromatids on chromosome dynamics. Related to Figure 4. Comparison of distribution of kinetochore motion stages (A) and velocity (B) during in HeLa cells (3xGFP-CENP-A, 3xGFP-centrin) during untreated Metaphase or Anaphase (n=10 each), after cohesin subunit SCC1 RNAi (n=13) or Laser ablation (n=29).

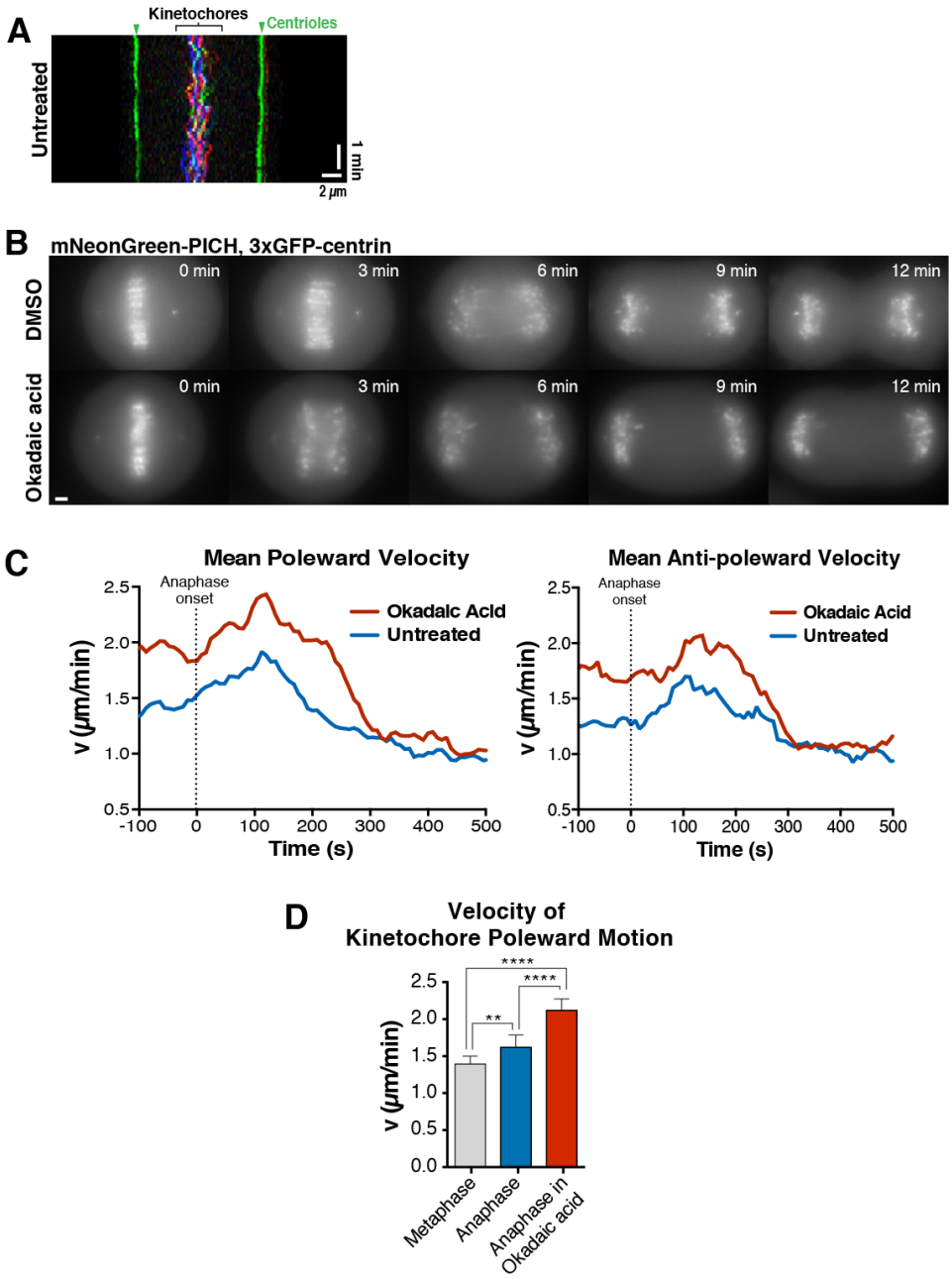

Figure S3. Effects of Okadaic acid on anaphase cell behavior and comparison to metaphase. Related to Figure 3. (A) Color-coded metaphase kymograph of an untreated (left n=10) HeLa cell (3xGFP-CENP-A, 3xGFP-centrin). (B) Representative time-lapse stills (maximal intensity projections) of HeLa cells expressing mNeonGreen-PICH, 3xGFP-centrin entering anaphase in presence of DMSO (upper row, n=10) or Okadaic acid (lower row, n=8). (C) Graphs showing distribution of motion stages, the average poleward velocity (left) or anti-poleward velocity (right) in untreated HeLa cells or Okadaic acid treated HeLa cells (3xGFP-CENP-A, 3xGFP-centrin) over time (n=10 cells each). (D) Comparison of distribution of anti-poleward motion in metaphase cells, untreated anaphase, or Okadaic acid-treated anaphase HeLa cells (3xGFP-CENP-A, 3xGFP-centrin; n>10 each; Unpaired t test results: **** $p<0.0001$, ** $p=0.0017$). Scale bars, 2μm.

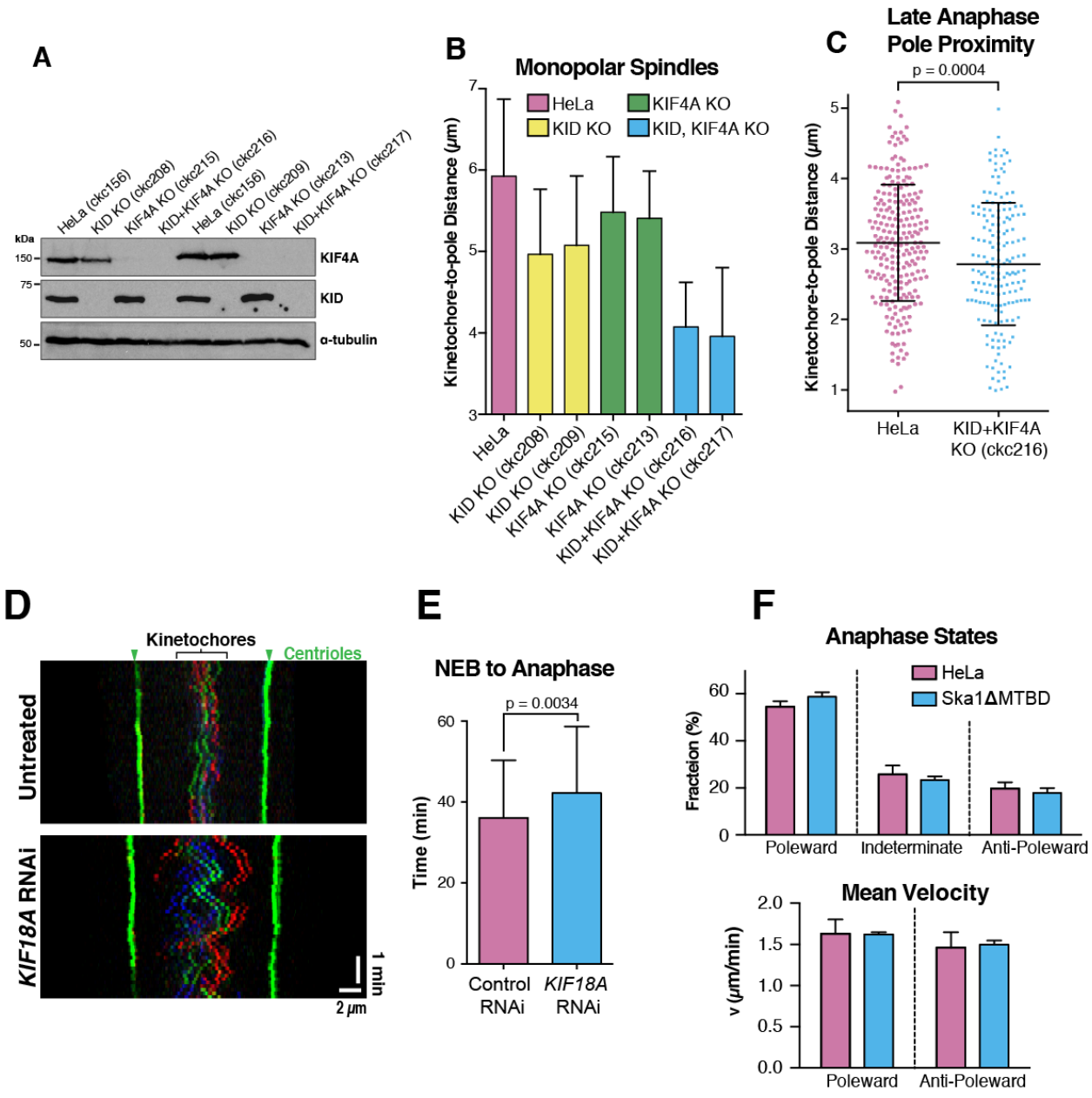

Figure S4. Characterization of Cell lines and Perturbations. Related to Figure 4. (A) Western blots probed for KIF4A, KID and *α*-tubulin (as a loading control) for HeLa cells (3xGFP-CENP-A, 3xGFP-centrin) in which the chromokinesins KID and/or KIF4A were eliminated using CRISPR/Cas9-mediated gene editing approaches. Asterisks indicate cells lines used in this study. (B) Kinetochore to pole distance in STLC treated cells with monopolar spindles (n>20 cells each). 2 independent single and double knock out cell lines of KID, KIF4A were compared to their progenitor HeLa cell line (3xGFP-CENP-A, 3xGFP-centrin). Error bar indicate standard deviation (C) Distribution of kinetochore to pole distance between control cells and KID, KIF4A double knock out HeLa cells (3xGFP-CENP-A, 3xGFP-centrin) 6 minutes after anaphase onset (n>174 kinetochores each pooled from 7 cells). Lines indicate average and standard deviation. P indicates

unpaired t test result. (D) Representative color-coded metaphase kymograph of an untreated (n=10) HeLa cell (3xGFP-CENP-A, 3xGFP-centrin) or treated with siRNA against KIF18A after 48h (right n=20). (E) Average nuclear envelope breakdown (NEB) to anaphase duration of cells after Control (n=104) or KIF18A (n=114) RNAi. P indicates unpaired t test result. (F) Comparison of relative ratio of states and velocity between untreated HeLa cells (n=10) and cells expressing Ska1-dMT mutant (n=5) after depletion of the endogenous protein.

Supplemental Movie Legends

Movie 1. **Anaphase chromosome dynamics in human cells.** Related to Figure 1. (Left) Untreated HeLa and hTERT RPE-1 cells (both expressing 3xGFP-CENP-A, 3xGFP-centrin) undergoing anaphase. t=0 was set to anaphase onset, 8 s intervals. (Right) Untreated HeLa cell (3xGFP-CENP-A, 3xGFP-centrin) imaged from metaphase to kinetochore release (with the stages indicated). t=0 was set to anaphase onset, 10 s intervals.

Movie 2. **Physical connections between sister chromatids are not required for anti-poleward motion.** Related to Figure 2. HeLa cell (3xGFP-CENP-A, 3xGFP-centrin) after cohesin (RAD21) depletion (upper left) at 8 s intervals, after kinetochore laser ablation (upper right) at 5 s intervals, displaying monopolar spindles induced by STLC treatment alone (bottom left) or additionally treated with MPS1i (bottom right) at 8s intervals. Boxes indicate tracked centrioles (green) or kinetochores displayed in figure graph. t=0 was set to beginning of movie.

Movie 3. **Perturbing the cellular phosphorylation state induces anaphase anti-poleward chromosome motion.** Related to Figure 3. HeLa cells (3xGFP-CENP-A, 3xGFP-centrin) untreated (upper left), in Okadaic acid (bottom left), expressing wild type (upper right) or non-degradable (bottom right) Cyclin B. t=0 was set to anaphase onset, 8 s intervals.

Movie 4. **Chromosome and kinetochore-derived forces contribute to anaphase anti-poleward motion in Okadaic acid-treated cells.** Related to Figure 4. HeLa cells (3xGFP-CENP-A, 3xGFP-centrin) either untreated, after KIF18A RNAi (+MPS1i), in the KID+KIF4A knockout, or following Ska1 replacement with a Ska1 ΔMTBD mutant (+MPS1i) treated with DMSO or Okadaic acid. t=0 was set to anaphase onset, 8 s intervals.

Table S1. Parameters of Anaphase Spindle and Kinetochore Motion. Related to Figure 1.

Cell Type	Anaphase Spindle Length		Maximum Pole Separation Speed	
	Early	Late	Velocity	Reached at Time After Anaphase Onset
HeLa	~12 µm	~20 µm	2.7 ± 0.6 µm/min	~1 min
hTERT-RPE1	~12 µm	~19 µm	2.6 ± 0.6 µm/min	~1.3 min

Cell Type	Anaphase Kinetochore to Pole Distance		Averaged Maximum Kinetochore to Pole Motion	
	Early	Late	Velocity	Reached at Time After Anaphase Onset
HeLa	6.13 ± 0.2 µm	3.2 ± 0.3 µm	1.17 ± 0.2 µm/min	~2 min
hTERT-RPE1	5.9 ± 0.6 µm	3.1 ± 0.6 µm	2.04 ± 0.7 µm/min	~0.66min

Cell Type	Early Anaphase (240s HeLa, 152s hTERT-RPE1)				
	Poleward State	Average Poleward Motion Speed	Pause State	Anti-poleward State	Average Anti-poleward Motion Speed
HeLa	54.5±2.4%	1.63±0.17 µm/min	25.8±3.8%	19.8±2.6%	1.46±0.19 µm/min
hTERT-RPE1	62.6±4.2%	2.03±0.16 µm/min	17.7±2.5%	19.7±3.6%	1.76±0.20 µm/min

Table S2. Kinetochore Dynamics of HeLa Cells. Related to Figure 1-4.

Condition (Number of Cells)	Frequency of State (%)			Velocity (µm/min)	
	Poleward	Indeterminate	Anti-poleward	Poleward	Anti-poleward
Untreated Metaphase (10)	33.1±2.0	34.2±2.9	32.7±2.9	1.39±0.11	1.25±0.08
Untreated Anaphase (10)	54.5±2.4	25.8±3.8	19.8±2.6	1.63±0.17	1.46±0.19
Prometaphase: *RAD21* RNAi (13)	33.7±4.6	22.2±6.5	44.1±8.3	2.27±0.39	1.66±0.21
Laser Ablation: First 20s (29)	69.0±24.7	18.1±21.0	12.9±18.4	3.50±1.11	2.45±1.08
Laser Ablation: After 20s (29)	40.3±7.8	24.7±9.1	35.0±10.3	2.96±0.76	2.48±0.60
Anaphase in Okadaic Acid (18)	52.6±4.4	17.6±2.1	29.8±5.3	2.04±0.18	1.84±0.10
Anaphase of *KID+KIF4A* KO in Okadaic Acid (12)	57.0±5.4	18.1±3.5	24.8±5.9	2.01±0.27	1.68±0.18
Anaphase of *KIF18A* RNAi in Okadaic Acid (5)	49.5±3.5	14.5±2.6	35.9±4.8	2.62±0.31	1.91±0.22
Anaphase of SKA1-ΔMTBD in Okadaic Acid (5)	46.4±8.6	32.4±7.1	21.1±8.5	1.54±0.24	1.20±0.21
Untreated Anaphase of SKA1- ΔMTBD (5)	58.8±1.9	23.4±1.5	17.9±2.0	1.62±0.03	1.50±0.05

Supplemental Datasets

Velocity distributions. Related to Figure 1, 3 and 4. Cell-to-cell heterogeneity of measured velocities for indicated conditions and total number steps of displacement displayed. Shown are the distributions of instantaneous poleward (positive values) and anti-poleward velocities (negative values) for every anaphase frame within the window used for calculations of all trajectories within a particular cell as determined from the trajectory annotations and displacements. Orange lines and label indicate average value and standard deviation.

TrackFiles.ZIP. Related to Figure 1-4**.** Document containing all .mdf files of every cell tracked in this study.

Supplemental Experimental Procedures

Cell Lines Used in This Study

ckc156: HeLa - 3xGFP-CENP-A, 3xGFP-centrin

ckc094: hTERT RPE-1 - 3xGFP-CENP-A, 3xGFP-centrin

ckc152: HeLa - mNeonGreen-PICH, 3xGFP-centrin

ckc208: HeLa3xGFP-CENP-A - 3xGFP-centrin, *KID* knockout

ckc209: HeLa3xGFP-CENP-A - 3xGFP-centrin, *KID* knockout

ckc213: HeLa3xGFP-CENP-A - 3xGFP-centrin, *KIF4A* knockout

ckc215: HeLa3xGFP-CENP-A - 3xGFP-centrin, *KIF4A* knockout

ckc216: HeLa3xGFP-CENP-A - 3xGFP-centrin, *KID* knockout, *KIF4A* knockout

ckc217: HeLa3xGFP-CENP-A - 3xGFP-centrin, *KID* knockout, *KIF4A* knockout

ckc101: HeLa3xGFP-CENP-A - 3xGFP-centrin, mCherry-Ska1-WT (hardened)

ckc103: HeLa3xGFP-CENP-A - 3xGFP-centrin, mCherry-Ska1-ΔMTBD (hardened)

Laser microsurgery

Single kinetochores were ablated by eight consecutive pulses (10 Hz repetition rate; pulse width: 8-10 ns; pulse energy: 1.5-2 μJ) derived from a doubled-frequency Elforlight laser (FQ-500-532) mounted on an inverted microscope (TE2000U; Nikon) equipped with a CSU-X1 spinning-disk confocal head (Yokogawa Corporation of America). Cells were imaged using a 100x 1.4 NA Plan-Apochromatic differential interference contrast objective (Nikon). Images were detected with an iXonEM+ EM-CCD camera (Andor Technology), using the NIS-Elements software (Nikon Instruments Inc.).

Image processing

Time-lapse images of 3xGFP-CENP-A cell lines were background subtracted (rolling ball radius: 2 pixels), sum projected and brightness/contrast adjusted in ImageJ/Fiji before further processing or analysis. Generation of kymographs was performed as described previously (Pereira and Maiato, 2010). Briefly, guided-kymographs were generated after manual spindle pole tracking, the coordinates of which were used to compensate for spindle rotation and translation over time, thereby stabilizing a virtual equator in the horizontal center of the kymograph. To collapse the kymograph, a routine was used that assigns an RGB color gradient to the vertical axis of each kymograph frame.

Analysis of kinetochore motion

All computational analyses of particle trajectories and the downstream analysis of kinetochore motion were performed using MATLAB 2014a. Single-particle trajectories (SPTs) of kinetochore motion were generated from sequential spatial localizations using the MTrackJ software package (Meijering, 2006) provided in Fiji/ImageJ. Individual kinetochore localizations were obtained manually using centroid fitting with a 9x9 pixel grid. Care was taken to avoid invalid assignments in which one kinetochore trajectory was connected with an unrelated kinetochore trajectory. With this in mind, merging and splitting events (two objects overlapping/separating), as well as gap closing connecting objects that disappear and reappear in a later frame (Jaqaman et al., 2008) were forbidden to eliminate the chances of these occurrences. In cases where there was

uncertainty in sequential particle localizations between two frames, trajectories were terminated.

To determine the localization error associated with estimated kinetochore positions, HeLa cells were fixed (10 min in 4% formaldehyde) and static kinetochores were imaged using the same imaging protocol that was applied to live cells. Kinetochores were tracked using the same parameters in MTrackJ (centroid fitting) to generate time-series single particle trajectories of stationary kinetochores. Motions of individual points along each trajectory were assumed to be due solely to independent localization errors, excluding stage drift and thermal motion. Under this assumption, the spatial localizations of individual particles can be modeled as distributed according to a Gaussian with the mean centered on the true (fixed) particle position and a standard deviation that is equal to the localization error. Figure S1C shows the localization error and fitting procedure for a single example kinetochore, where σ_e is the localization error associated with the normal distribution fit to the sequential localization measurements. Analyses of eighteen such trajectories of stationary kinetochores were performed with their localization errors individually computed in this manner (Figure S1D). The overall distribution from compiling the individual localization errors for each trajectory estimated in this manner was then used to obtain the final mean-value estimate of the localization error that was subsequently used for classification of kinetochore motion behaviors (34.2 ± 5.8 nm; mean ± s.d.). Kinetochores and spindle poles were assumed to have equal localization errors.

To classify poleward and anti-poleward moving kinetochores (Figure S1F), we analyzed the single-step-level dynamics of individual kinetochore trajectories.

Kinetochore trajectories were assigned to their corresponding spindle poles based on the minimum mean distance during anaphase. In KIF18A-depleted cells, chromosomes do not align to form a proper metaphase plate, so the assignment of the corresponding spindle pole was based on the minimum distance of the last tracked frame for the kinetochore in question. The time of anaphase onset for each individual cell was defined as the time point immediately prior to the separation of sister chromatid populations as annotated manually using visual inspection based on the distance between the kinetochore-spindle pole groups. For anaphase motion, we analyzed the first 240 seconds in HeLa cells or 152 seconds in hTERT-RPE1 cells after anaphase onset. For metaphase, we analyzed motions of the first 320 seconds of a >600 second movie in which the cell remained in metaphase throughout the imaging process.

After the assignment of kinetochores to spindle poles, the change in distance (displacement) between each kinetochore and their corresponding spindle poles was computed over time. Measurements of these displacements will be slight underestimates due to the possibility of out-of-plane motion that is lost in projection of kinetochore and spindle pole positions to the imaging plane. Displacements were then analyzed to determine whether a kinetochore was moving poleward or anti-poleward. Note that to classify poleward/anti-poleward motion based on the change in distance between the kinetochore in question and its assigned spindle pole, the uncertainty in the distance, σ_D, between the two objects rather than simply the localization error, σ_e, of each object itself must be considered. This distance uncertainty is derived from the propagation of error in computing the distance from the localizations of the kinetochores and spindle poles, where the uncertainty in the distance is related to the localization

error by $\sigma_D = \sqrt{2}\sigma_e$. An event was defined as "indeterminate" if the kinetochore displacement (Δx) between two time points was smaller than $\sqrt{2}\sigma_D$. Adjusting this ad hoc threshold results in a trade-off between the detectability of kinetochore poleward/anti-poleward motions and the mis-assignment of localization noise to these motion states in the analysis.

Cell-to-cell heterogeneity in kinetochore displacement as well as velocity distributions were characterized following annotation of trajectories into poleward and anti-poleward states. Additionally, the percentage of time spent in each state across all kinetochores for each individual cell was computed over the anaphase period. The sample mean of each metric for each cell was used to compute the overall distribution of the metric for each condition or cell line. For the calculation of statistical significance between treatment conditions or perturbations, Prism 6 (GraphPad) was used to perform unpaired, two-tailed Student's t-tests. Independent samples tested represent measurements from distinct cells in a given condition, with the set of individual trajectories per cell contributing to the mean behavior for that cell. At least five independent samples were analyzed in each case. To highlight this point, distributions of both poleward and anti-poleward velocities were plotted for each cell and are consistent within their groups. The cell-by-cell distributions of velocities for cells analyzed in Figures 1, 3 and 4 can be found in the Supplemental Dataset along with the complete data set from our tracking of each individual cell and condition as both MATLAB .mat data files as well as MTrackJ .mdf trajectory files.

We additionally evaluated the sensitivity of classified kinetochore behaviors to imaging frame rate, including the classification of poleward versus anti-poleward motion

and their associated state lifetimes. For this analysis, untreated HeLa cell kinetochore trajectories obtained using 4 seconds/frame imaging conditions were “coarsened” computationally to decrease sampling to 8 and then 12 seconds/frame by omitting data from neighboring time-points. Results indicate that trajectory coarsening results in an overall increase in displacement magnitude between successive frames, as expected for a random process with drift (Figure S1F; Berg, 1993; Monnier et al., 2015; Monnier et al., 2012). Accordingly, a smaller fraction of kinetochore displacements is classified as “indeterminate” (Figure S1E) because more displacements per trajectory exceed the localization error threshold. Associated estimations of the lifetimes of individual motion states are also observed to depend strongly on sampling frequency because of the similar dependence of active versus diffusive transport on the time-scale of observation. Thus, the local lifetime of a given poleward/anti-poleward processive motion depended strongly on sampling frequency, and was omitted from analysis.

An example “coarsened” (4s, 8s, 12 s/frame) trajectory is shown in Figure S1F. This trajectory is annotated in color using its “state sequence” corresponding to the intervals that the algorithm has classified as poleward, anti-poleward, or indeterminate. At 4 s/frame, a large fraction of the intervals annotated fall below the minimum threshold for labeling a particular displacement as poleward or anti-poleward. This is due to the average step size that the kinetochore moves during the 4 second interval falling near or below the detection threshold that is imposed by the localization error. Decreasing temporal resolution (4 s/frame to 8 s/frame) results in larger displacements, leading to more intervals that are positively annotated as having motion beyond the noise threshold. Trajectories can be coarsened further (8 s/frame to 12 s/frame) at the cost of

decreased temporal resolution, which may result in the failure to detect motion dynamics on faster timescales. Given this sensitive dependence of motion state lifetimes on sampling frame rate, we refrained from reporting motion state lifetime information.

Supplemental References

Berg, H. (1993). Random Walks in Biology Princeton University Press. Princeton, NJ, 30.

Jaqaman, K., Loerke, D., Mettlen, M., Kuwata, H., Grinstein, S., Schmid, S.L., and Danuser, G. (2008). Robust single-particle tracking in live-cell time-lapse sequences. Nature methods *5*, 695-702.

Meijering, E. (2006). MTrackJ: A Java program for manual object tracking. University Medical Center Rotterdam,[Online] Available: http://wwwimagescienceorg/meijering/software/mtrackj.

Monnier, N., Barry, Z., Park, H.Y., Su, K.C., Katz, Z., English, B.P., Dey, A., Pan, K., Cheeseman, I.M., Singer, R.H.*, et al.* (2015). Inferring transient particle transport dynamics in live cells. Nature methods *12*, 838-840.

Monnier, N., Guo, S.M., Mori, M., He, J., Lenart, P., and Bathe, M. (2012). Bayesian approach to MSD-based analysis of particle motion in live cells. Biophys J *103*, 616-626.

Pereira, A.J., and Maiato, H. (2010). Improved kymography tools and its applications to mitosis. Methods *51*, 214-219.